Iraqi Journal of Physics, 2025 *Vol.23, No.3, PP.149-163*
https://doi.org/10.30723/ijp.v23i3.1397 *P-ISSN: 2070-4003*
E-ISSN: 2664-5548

Improvement of Image Fusion Using Multi-Resolution Color Images

Woroud F. Ahmed[1*] and Mohammed I. Abd-Almajied[2]
[1]*Department of Remote Sensing and GIS, College of Science, University of Baghdad, Baghdad, Iraq*
[a*]Corresponding author: wurud.firas2209m@sc.uobaghdad.edu.iq

Abstract
The image fusion technique was employed to generate a high-resolution image from a low-resolution one. A high scale was achieved by increasing the resolution of an image through interpolation, which relies on pixel neighbours. Multispectral images (low-resolution images with high resolution) from different satellites were utilized in this work for obtaining a high-resolution image. The crucial part of image fusion is image registration, which depends on obtaining a good high-resolution image. A scale-invariant feature transform (SIFT) was utilized to receive control points with an affine transform. Correct control points are determined depending on the scale of the image (downscaling followed by upscaling), which is necessary for stabilizing match control points between images. Control points were identified using the SIFT algorithm, which utilizes distance and angle to determine the correct match points. A different scale image is used to detect and correspond to the correct control points between the two images, thereby speeding up the process. Also, image scaling with contrast stretching was utilized for preprocessing to stretch brightness to obtain high-quality image features. A morphological operation is applying post-processing to images (scale, contrast stretching, and radiometric operation). Final image fusion is obtained using the colour model (luminosity, hue, and saturation). A metric criterion, root mean square error (RMSE), with peak signal-to-noise ratio (PSNR) is utilizing for determining the goodness of this process, which is used in image fusion.

Article Info.

Keywords:
Image Fusion, High Resolution Image, Low Resolution Image, Multi Spectral Image, Image Matching.

Article history:
Received: Nov. 11,2024
Revised: Jan. 31, 2025
Accepted: Feb. 01, 2025
Published: Sep. 01, 2025

1. Introduction
Remote sensing technology is essential for detecting and identifying objects. There are two types of objects: visible objects, such as land cover, and invisible objects, such as temperature, evaporation, and salinity. A visible object can be seen with the eye, but a sensor is needed to identify the invisible object [1]. Satellite images of remote sensing are widely used in many applications, such as GPS, remote sensing, disaster management, etc. Although a satellite image provides accurate data about the Earth, their analysis could be complex, necessitating pre-processing. Enhancing resolution is one of the most important steps in image accuracy [2]. Image enhancement works on the sensitivity of information in improved input image processing methods. Enhancement is divided into two approaches in the frequency and spatial domains [3]. It could increase the accuracy of the information by merging data from multiple sensors to improve spatial detail and feature information. Data fusion technology is an effective technique for producing images with different spatial and spectral resolutions from different satellites [4-6]. The fusion technique reconstructs a low spatial resolution image using a high spatial resolution image to produce the same pixel size [7-9].

There are different challenges: Geometric Distortions [10] due to different devices (sensors) in direction, scale and perspective, so that image registration was the appropriate and accurate process to match the features correctly [11]; and temporal differences, might become more difficult if images captured at different times that reveal changes in the scene. The idea of different of spatial resolutions of image satellites was made by combining images of different resolutions, especially when trying to preserve details from a high-resolution image. Also, it could preserve sensor characteristics (such as intensity variations and sensor noise), data quality, and restore data gaps [12].

Different studies were reported concerning this topic. In 2004, Dufournaud et al. created a method for solving the problem of matching two images (one of high resolution and the second of low resolution). They built a system that allowed comparing two images with different resolutions and extracting points of interest at various scales up to 6 scales. The important challenge in this study was that only images of different resolutions, scaling, and geometric mismatch could be matched [10].

In 2010, Lin et al. produced a new algorithm for image registration based on the Harris operator and affine transform. It was shown that the resulting method was effective and correct. There were challenges in improving the accuracy of the angles, reducing the effect of noise, and improving the matching [13].

In 2014, Zhu and Ren proposed a new method based on Harris detection with a scale invariant feature transform (SIFT) feature with a direct line segment. A RANSAC was used for filtering control points. The method had strong robustness for rotation, resolution, scaling and lighting. It could acquire more accurate matching pair points and improve the quality of image mosaics. This study faced many challenges, the most important of which were changes in lighting and resolution, scaling, rotation, and noise. Even lighting with more accurate matching control points could be avoided using description of directed line segment with SIFT feature [14].

In 2023, Shaharom and Tahar carried out a study of the performance of SIFT and SURF (Speeded-Up Robust Features) algorithms on multispectral images, especially those that include greater than three bands. A less visibility of features in these images may lead to nonlinear intensity between images. A proposed method for solving this problem was carried out by the combination of various descriptors and revision or alteration within the algorithm to achieve a good result in image fusions [15].

In this research, a new image fusion technique was carried out using two images (high resolution and low resolution) of the same scene from Landsat 8 and Sentinel-2 satellites. The idea of this work is to apply a color model to produce a final fusion image. Luminosity, hue and saturation bands were the crucial features of this color model. Beyond color model, there were some steps which were necessary for doing this work (e.g., image registration that based on the SIFT detection and affine transformation model). Image registration was carried out under some conditions, such as scale which affects the choosing of control points for image registrations. Also, some methods of image enhancement (contrast stretch, histogram and image morphology) were necessary for brightness calibrations. The final image with high resolution was obtained by utilizing a color model. The paper's layout is as follows: section two showed the study area, and section three illustrated the methodology. Results and discussion are shown in section four, and finally, conclusions with future work are presented in section five.

2. Study area and Data Set

The Landsat 8 satellite is part of the Landsat data continuity mission, a collaborative initiative between NASA and the United States geological survey (USGS). In this study, two satellite images were employed. The first image was acquired from the Landsat 8 operational land imager (OLI) sensor, covering path 169, row 037, on (June 19, 2023), as seen in Table 1. The OLI bands (band 4, band 3, band 2) were downloaded from the USGS platform.

The second image was obtained from the Sentinel-2 satellite, which was part of the European space agency (ESA) mission developed under the framework of the European Union's Copernicus program. The datasets used in this research are illustrated in Fig. 1. The Sentinel-2 image, selected for its higher spatial accuracy of up to 10 meters, was acquired on (June 22, 2023), as seen in Table 1. Band 2, Band 3, and Band 4 were

downloaded from the Copernicus Open Access Hub (scihub.copernicus.eu). Table 2 shows the specifications of the two satellites.

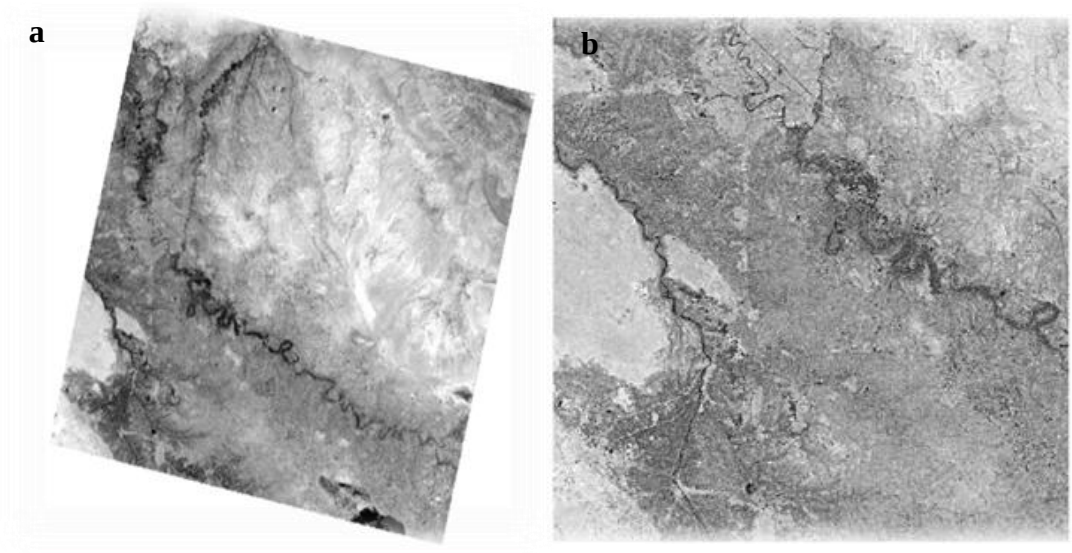

Figure 1: The study area: (a) Landsat 8 OLI sensor, (b) Sentinel-2 satellite images.

Table 1: The satellite image of the study area.

	Landsat 8	**Sentinel 2**
Acquired Date	2023/6/19	2023/6/22
Longitude	(44 15′55″) to (44 17′38″) E	(44 15′55″) to (44 17′38″) E
Latitude	(33 25′46″) to (33 24′21″) N	(33 25′46″) to (33 24′21″) N
Resolution	30 m	10 m

Table 2: Spectral bands range and spatial resolution of Sentinel-2A MSI and Landsat 8 OLI sensors of the area study.

	Landsat 8 OLI			**Sentinel 2**		
Band	**Spectral region**	**Wavelength range**	**Resolution**	**Spectral region**	**Wavelength range**	**Resolution**
B2	Blue	452-512	30	Blue	458-523	10
B3	Green	533-590	30	Green Beak	543-578	10
B4	Red	636-673	30	Red	650-680	10

3. Methods

The flow-chart of this work is shown in Fig. 2.

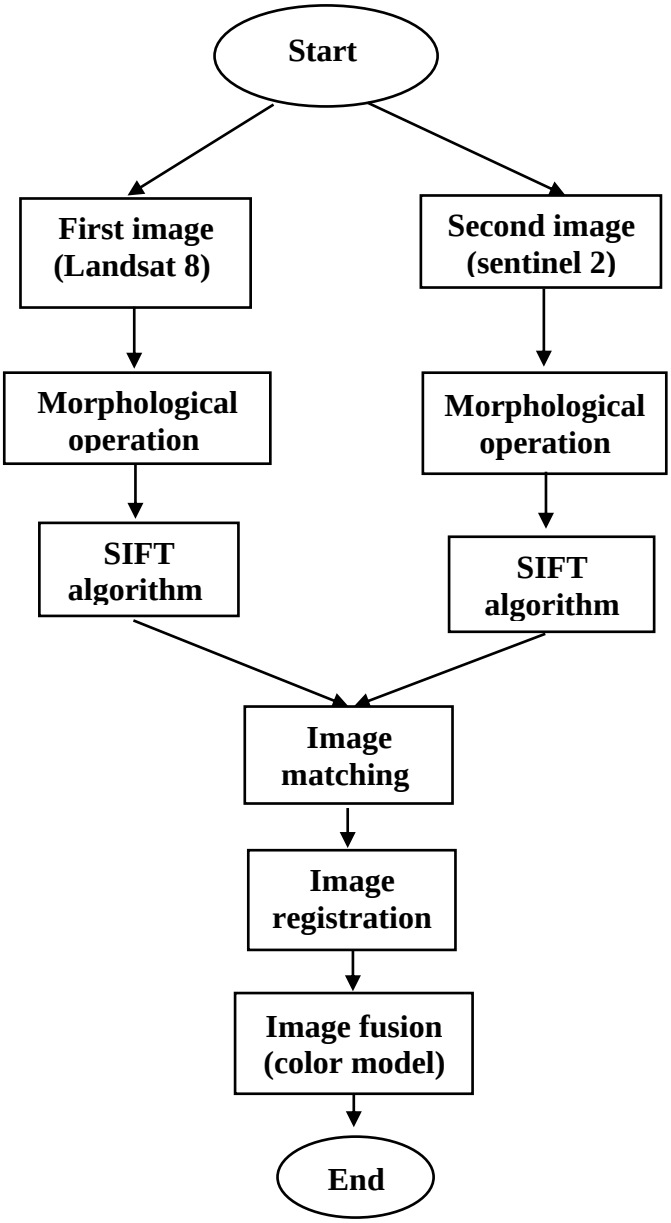

Figure 2: Flow chart of the work.

3. 1. Scale Image

Image resizing is essential in many applications, such as image processing applications. The size of the image is changed while maintaining the important features intact. Changing the scale of the image is done by reducing or increasing the number of pixels, which affects the accuracy and details of the image [16]. The number of pixels that could be generated from the initial pixels in an image could be increased using various techniques. A technique frequently used is the algorithm for image interpolation. There were several types of interpolation: Bicubic Interpolation, Bilinear Interpolation, and Nearest Neighbour [17].

3. 2. SIFT Detection

A matching was created between two images by detecting the key points in the two images using the SIFT detection technique for local feature detection, which was initially proposed by D. Lowe [18], through Eq. (1) [19]. The main idea was based on the Gaussian function. The following equation represents the scale space of 2-dimension

$$L(x, y, \sigma) = G(x, y, \sigma) \times I(x, y) \quad (\mathbf{1})$$

where L(x, y, σ) is the scale space, G (x , y , σ) is the variable-scale Gaussian, I(x, y) is the input image, σ is the Gaussian standard deviation, and * is the convolution operator.

The Gaussian function is

$$G(x, y, \sigma) = \frac{1}{2\pi\sigma^2} e^{-\left(\frac{x^2+y^2}{2\sigma^2}\right)} \quad (\mathbf{2})$$

$$D(x, y, \sigma) = \big(G(x, y, k\sigma) - G(x, y, \sigma)\big) \times I(x, y) \quad (\mathbf{3})$$

$$= L(x,y,k\sigma) - L(x,y,\sigma)$$

To find the matching between two images, a criterion was utilized and applied between the control points, which resulted from Eq. (3). Eqs. (4) and (5) were used to extract the correct key points in the two images by distance and angle [16, 20].

$$\theta = \tan^{-1}\frac{y}{x} \quad (\mathbf{4})$$

where y represents i raw, and x represents the j raw

$$\text{diff} = \Delta d + \frac{\Delta\theta}{\Delta\delta} \quad (\mathbf{5})$$

where Δd represents the differences between the distance (for first and second images), Δθ represents the differences between two angles of the images, Δδ represents the deflection of each angle if it was near or far from the reference point.

3. 3. Preprocessing

Contrast stretching is an essential technique in image processing. It was used to improve the visibility of features in the two images using standardization through Eq. (6) [12].

$$\overline{x} = \frac{x-\mu}{\sigma} \quad (\mathbf{6})$$

where (μ) represents the mean and (σ) is the standard deviation.

The mean was calculated through Eq. (7) and (8) [21].

For the x-axis

$$x_i = \frac{1}{N}\sum_{k=1}^{N} x_k \quad (\mathbf{7})$$

For the y-axis

$$Y_i = \frac{1}{N}\sum_{k=1}^{N} y_k \quad (\mathbf{8})$$

where N is the size of columns in the x-axis and the size of rows in the y-axis.

3. 4. Affine Transformation

Affine transformation is used in image processing to align two images. An affine transformation, also called an affinity, preserves proportions on lines; it does not necessarily preserve angles or lengths [22]. The behaviour of this transformation is transforming parallel lines to parallel lines. The matrix form is [23]

$$\dot{x} = ax + by + c \quad (\mathbf{9})$$

$$\dot{y} = bx + ay + d \quad (\mathbf{10})$$

$$\begin{bmatrix} x \\ y \\ 1 \end{bmatrix} = \begin{bmatrix} 1 & 0 & h \\ 0 & 1 & k \\ 0 & 0 & 1 \end{bmatrix} \begin{bmatrix} \cos\theta & -\sin\theta & 0 \\ \sin\theta & \cos\theta & 0 \\ 0 & 0 & 1 \end{bmatrix} \begin{bmatrix} s & 0 & 0 \\ 0 & s & 0 \\ 0 & 0 & 1 \end{bmatrix} \begin{bmatrix} 1 & \alpha & 0 \\ \beta & 1 & 0 \\ 0 & 0 & 1 \end{bmatrix} \quad (\mathbf{11})$$

where h, k are the translation parameters, h is the horizontal shift, k is the vertical shift, S represents the scaling factor, and α, β represent the shear factor, where α controls the horizontal skew and β controls the vertical skew.

The general form of transformation matrix is expressed by Eq. (9) and (10) or in matrix form

$$x' = a_{11x+}a_{22+} \quad (\mathbf{12})$$

$$y' = a_{21x+}a_{22+}a_{23} \quad (\mathbf{13})$$

$$\begin{bmatrix} \dot{x} \\ \dot{y} \\ 1 \end{bmatrix} = \begin{bmatrix} a_{11} & a_{12} & a_{13} \\ a_{21} & a_{22} & a_{23} \\ 0 & 0 & 1 \end{bmatrix} \begin{bmatrix} x \\ y \\ 1 \end{bmatrix} \quad (\mathbf{14})$$

3. 5. Color Model

Colors are important for humans in communicating and identifying species (ex. Intensities, frequencies,…). These colors are represented numerically within a mathematical formula. This representation in mathematics is known as a color model that could represent the color space using the three main colors—blue, green, and red. The computer could visualize color and brightness. In these methods, redundancy between color components is reduced by converting the primary colors to an unrelated color model, such as YUV.

Luminance (Y channel) and two chrominance components (UV channels) represent the (YUV) color space. U shows the color difference between blue signal and luminance (B−Y) and V represents the difference between red, and luminance (R−Y). RGB values can be converted to YUV color space using Eq. (15), while using Equation (16) converts YUV to RGB [24].

$$\begin{bmatrix} Y \\ U \\ V \end{bmatrix} = \begin{bmatrix} 0.299 & 0.587 & 0.114 \\ -0.147 & -0.289 & 0.436 \\ 0.615 & -0.515 & -0.100 \end{bmatrix} \cdot \begin{bmatrix} R \\ G \\ B \end{bmatrix} \quad (\mathbf{15})$$

$$\begin{bmatrix} R \\ G \\ B \end{bmatrix} = \begin{bmatrix} 1.000 & 0.000 & 1.140 \\ 1.000 & -0.395 & -0.581 \\ 1.000 & 2.032 & 0.000 \end{bmatrix} \cdot \begin{bmatrix} Y \\ U \\ V \end{bmatrix} \quad (\mathbf{16})$$

3. 6. Root-Mean- Square Error

The Root-Mean-Square Error (RMSE) is a standard metric used in model evaluation. For a sample of n observations y (y_i, i=1,2,3,..n) and n corresponding model predications $\hat{y}$ [25, 26], the RMSE is

$$\mathrm{RMSE} = \sqrt{1/n \sum_{i=1}^{n} (y_i - \hat{y}_l)^2} \quad (\mathbf{17})$$

3. 7. Peak Signal-to-Noise Ratio (PSNR)

A theory was developed in (1980) to calculate the signal-to-noise ratio (SNR) of two images based on their cross-correlation coefficients [27]. The peak signal-to-noise ratio (PSNR) represents the similarity between two images. The two images have large numerical differences if the PSNR is low. Furthermore, PSNR has higher sensitivity than the structural similarity index. Therefore, to determine how comparable, two images are, the PSNR is computed.

Using Eq. (18) and the PSNR, the similarity between the two images was computed as follows [9, 28]

$$\mathrm{PSNR} = 10 \log_{10} \left(\frac{\mathrm{MAX}_I^2}{\mathrm{MSE}} \right) \quad (\mathbf{18})$$

where MAX_I represents the maximum fluctuation determined by the type of input image, and MSE represents the mean squared.

4. Results and Discussion

The first step was calculating the key points in the two images (Landsat-8 and Sentinel-2) using Eqs. (1-3). Depending on the match features between the images, as seen in Fig. 3, a reference point in the two images was established, as seen in Fig. 4. Matched points with the aid of Eqs. (4) and (5) between the two images are shown in Fig. 5. For complete best matching between images, a rescaling of the images was applied to obtain a reasonable result. Downscaling of the two images was applied first, and then a gradual upscaling to obtain the final result, as shown in Fig. 6. Also, the first-order derivative (affine transform), Eq. (14), was utilized to determine the effectiveness of the final match with the aid of radiometric.

Finally, the shared part of the two images was calculated using Eq. (14) and the rest of the image was ignored, as seen in Fig. 7. High-resolution image was found using a colour model that depends on luminosity, hue and saturation depending on Equations 15 and 16. Luminosity was used for the Sentinel image, and hue and saturation were used for the Landsat image. This model can find a reasonable result because most information holds in the luminosity part of the colour model. The results of the metric criterion represent the rate of loss of value when applying the colour model to the images. Root-mean-square error and peak signal-to-noise ratio were applied on images before fusion. Results of Eqs. (17) and (18) are listed in Table 3-6. Histograms of error value of the

images when applying the colour model on the images before using image fusion are shown in Figs. 12 and 13. They show the distribution of error around the zero value with width strength, which shows the goodness of the result (lighter better than thicker). The histograms in Fig. 10 (Landsat images) were broader in base than those in Fig. 11 (Sentinel images) because an image upscaling (using bicubic interpolation) was applied on Landsat images that may affect the results. This was mean a little wide error. A metric value was shown for the Landsat image as compared to the Sentinel image in Tables 3 and 4 for checking colour model quality. Table 5 and 6 were reveal these metric values after applying image fusion between Landsat and Sentinel image.

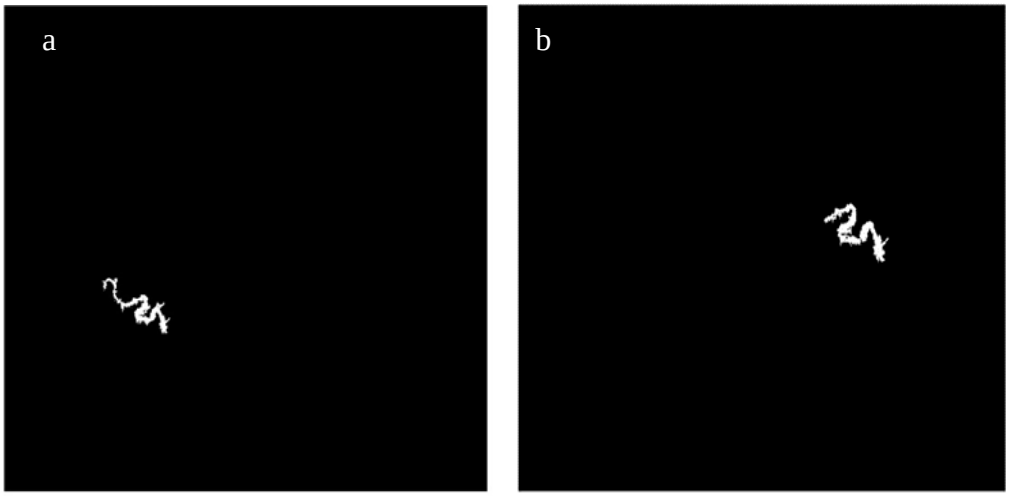

Figure 3: the match features of the two images, (a) Landsat image, (b) Sentinel image.

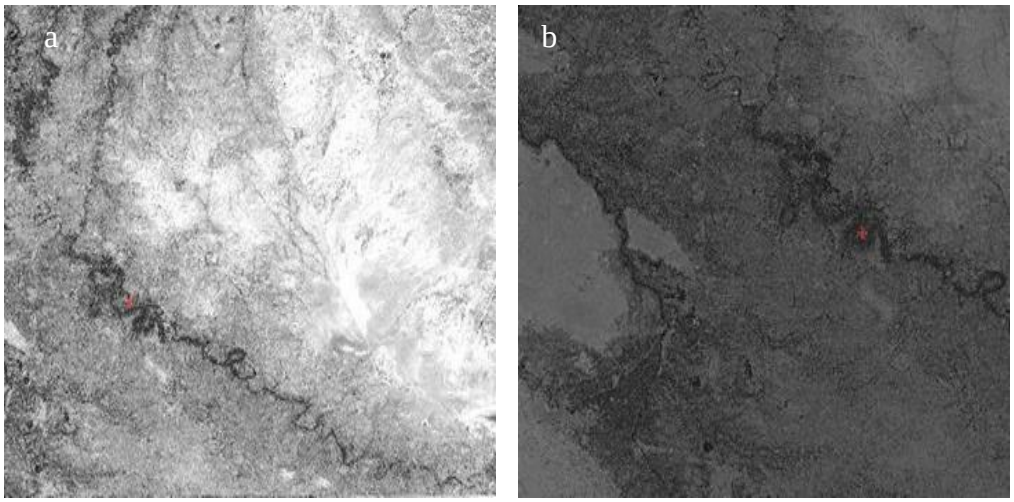

Figure 4: the reference point in two the images, (a) Landsat image, (b) Sentinel image.

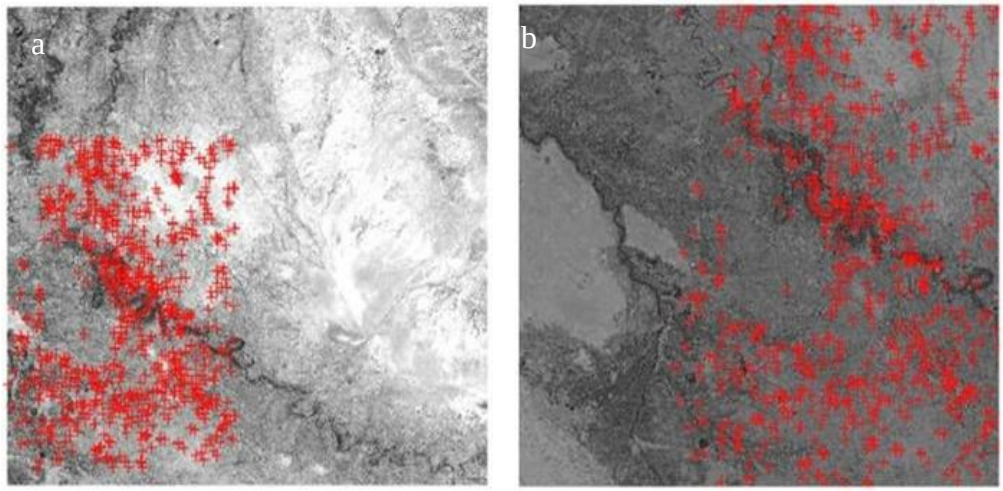

Figure 5: the match points in both images, (a) Landsat image, (b) Sentinel image.

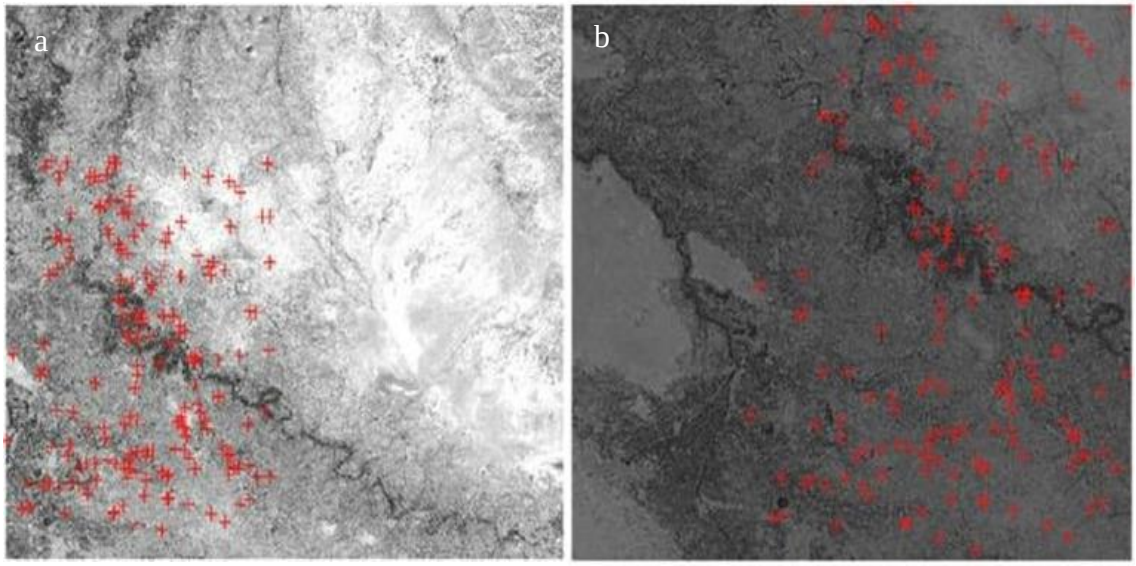

Figure 6: Second match corresponding between; a. Landsat b. Sentinel.

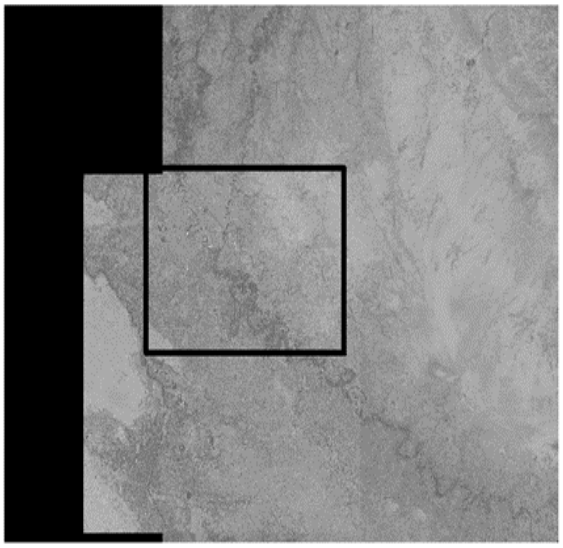

Figure 7: Share or interface area between the two images.

Figure 8: Final images.

Figure 9: Segments of final image.

Table 3: bands of Landsat before fusion.

Band Landsat	Mean-Square Error of Histogram	Root-Mean-Square Error	PSNR
Red	0.0098	1.3163	45.7440
Green	0.0080	0.9140	48.9115
Blue	0.0269	1.4113	45.1386

Table 4: Metrics of Sentinel.

Band Sentinel	Mean-Square Error of Histogram	Root-Mean-Square Error	PSNR
Red	0.0054	1.5981	44.0585
Green	0.0060	1.0230	47.9337
Blue	0.0080	1.3645	45.4311

Table 5: Metrics of hybrid with Landsat.

Band	Mean-Square Error of Histogram	Root-Mean-Square Error Landsat	Root-Mean- Square Error Sentinel	PSNR Landsat	PSNR Sentinel
Red	0.0131	45.9934	8.9250	14.8769	29.1186
Green	0.0076	46.2403	3.6018	14.8304	37.0004
Blue	0.0121	45.9987	11.9683	14.8759	26.5702

Table 6: Metrics of hybird with Sentinel.

Band	Mean-Square Error of Histogram	Root-Mean-Square Error Landsat	Root-Mean-Square Error sentinel	PSNR Landsat	PSNR sentinel
Red	0.0111	45.9934	8.9250	14.8769	29.1186
Green	0.0405	46.2403	3.6018	14.8304	37.0004
Blue	0.0146	45.9987	11.9683	14.8759	26.5702

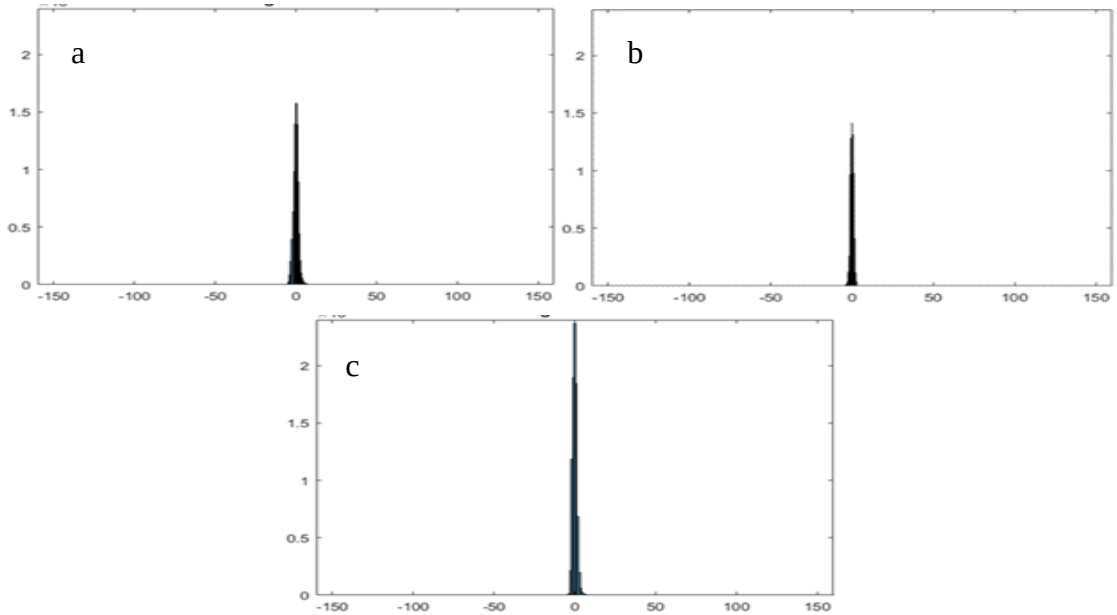

Figure 10: Histogram of error (Landsat image): (a)red band, (b)green band, (c)blue band.

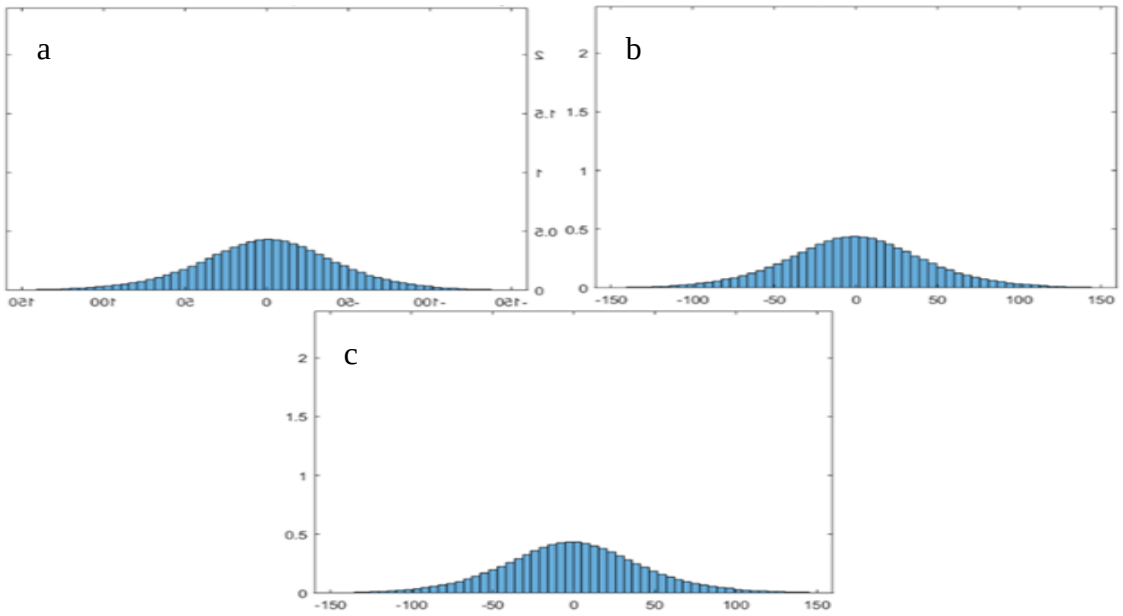

Figure 11: Histogram of error (Sentinel image): (a)red band, (b)green band, (c)blue band.

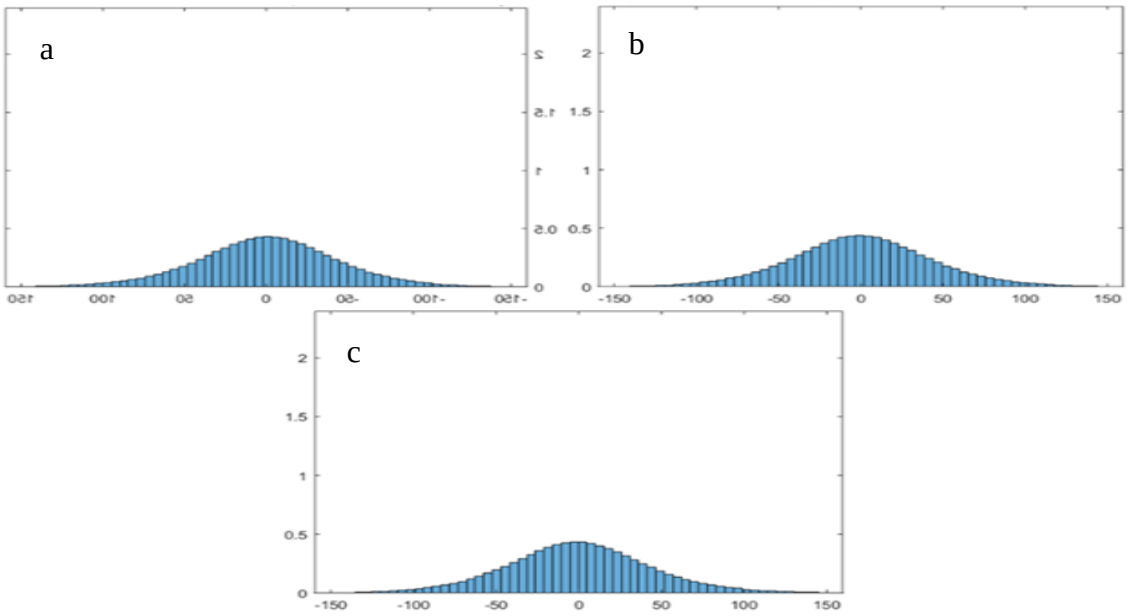

Figure 12: Histogram of error (hybrid with Landsat image): (a)red band, (b)green band, (c)blue band.

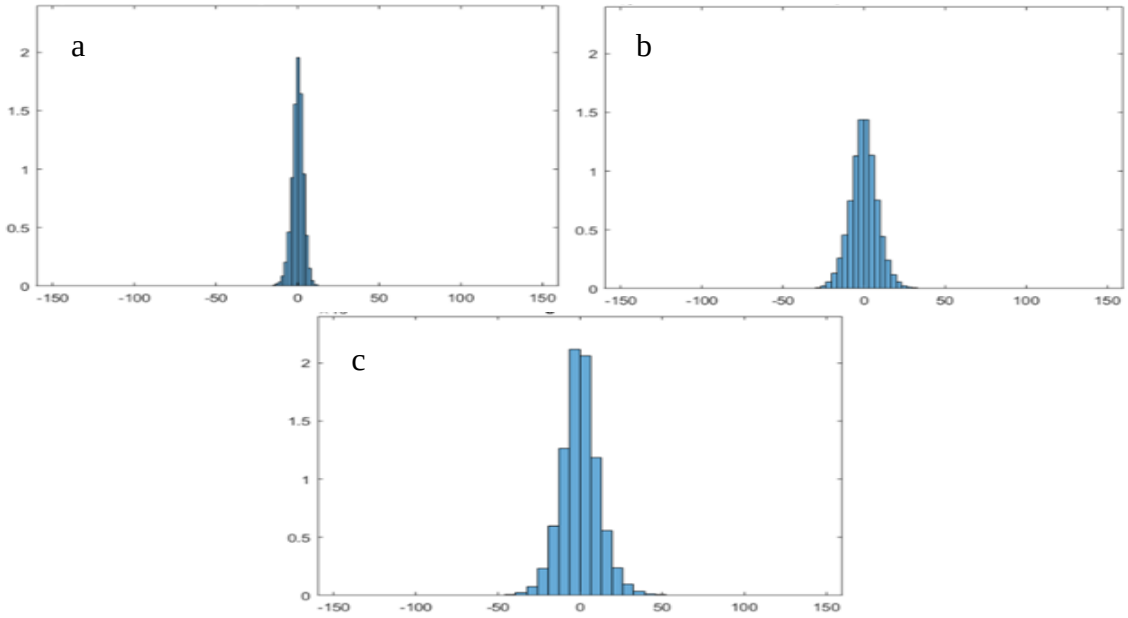

Figure 13: Histogram of error (hybrid with sentinel image): (a) red band, (b) green band, (c) blue band.

5. Conclusions

The goal of this work was to improve spatial resolution through image fusion. A good result may have been achieved depending on the best matching between images. Image registration was done on a scale match between images (downscale), because different scales affect the best image match (registration)—also, down sampling of the image accelerates the computing process. Radiometric was down in the final step with the original scale because the downscale used interpolation, which affects its result. Image preprocessing (contrast stretching, histogram equalization, and feature extraction) was necessary to obtain reference points, followed by the rest of the control points. An equation of deflections was essential for the correct shift control points. Image mosaic was done for selecting a matching area by using the first-order transformation (affine transform). Atmospheric conditions and the time of acquisition affect the quality of the final image, so it is captured at nearly the same time. RMSE and PSNR were utilized on images after applying the colour model. There were two sets of metric values. One set was obtained from the same satellite image, converted using the colour model (luminosity, hue, and saturation), and then back to RGB to find the percentage error. Secondly, the rest of the test was applied between the hybrid image (the enhanced one) and its original image. The alteration value of the metric criterion may differ between satellites because one satellite has a low resolution that is upscaled (increased resolution through interpolation) compared to another satellite with high resolution. A reasonable final fusion image was obtained from this work. The application of high image resolution or image fusion could be useful in urban planning, agricultural areas, and determining the amount of available water. Image fusion, depending on the wavelet transform, will be used in future work. Future work may also incorporate a hyperspectral image with multispectral data.

Conflict of Interest

Authors declare that they have no conflict of interest.

References

1. H. Lestiana and Sukristiyanti, IOP Conf. Ser. Earth Environ. Sci. **118**, 012047 (2018). https://doi.org/10.1088/1755-1315/118/1/012047.
2. L. Sharma, S. Sengupta, and B. Kumar, J. Phys.: Conf. Ser. **1714**, 012051 (2021). https://doi.org/10.1088/1742-6596/1714/1/012051.
3. I. M. Hayder, H. A. Younis, and H. Abdul-Kareem Younis, J. Phys.: Conf. Ser. **1279**, 012072 (2019). https://doi.org/10.1088/1742-6596/1279/1/012072.
4. S. Ashraf, L. Brabyn, and B. J. Hicks, Appl. Geog. **32**, 619 (2012). https://doi.org/10.1016/j.apgeog.2011.07.010.
5. H.-S. Jung and S.-W. Park, Sensors **14**, 24425 (2014). https://doi.org/10.3390/s141224425.
6. A. A. Hamed, A. Al-Safar, and N. A. Taha, Ibn AL-Haitham J. Pure Appl. Sci. **30**, 236 (2017). https://doi.org/10.30526/30.3.1624.
7. Y. Li, C. Huang, J. Hou, J. Gu, G. Zhu, and X. Li, Agricult. Fores. Met. **244-245**, 82 (2017). https://doi.org/10.1016/j.agrformet.2017.05.023.
8. A. A. N. Al-Jasim, T. A. Naji, and A. H. Shaban, Iraqi J. Sci. **63**, 4131 (2022). https://doi.org/10.24996/ijs.2022.63.9.40.
9. R. A. Abdulwahab, L. A. Al-Ani, and A. H. Shaban, AIP Conf. Proc. **3018**, 020009 (2023). https://doi.org/10.1063/5.0171974.
10. Y. Dufournaud, C. Schmid, and R. Horaud, Proceedings IEEE Conference on Computer Vision and Pattern Recognition. CVPR 2000 (Hilton Head, SC, USA IEEE, 2000). p. 612.
11. F. F. Sabins Jr and J. M. Ellis, *Remote Sensing: Principles, Interpretation, and Applications* (USA, Waveland Press, Inc, 2020).
12. M. I. Abd-Almajied, L. E. George, and R. S. Hameed, Iraqi J. Sci., 2635 (2023). https://doi.org/10.24996/ijs.2023.64.5.44.
13. H. Lin, P. Du, W. Zhao, L. Zhang, and H. Sun, 2010 3rd International Congress on Image and Signal Processing (Yantai, China IEEE, 2010). p. 2184.
14. J. Zhu and M. Ren, Comput. Math. Meth. Med. **2014**, 926312 (2014). https://doi.org/10.1155/2014/926312.
15. M. Shaharom and K. Tahar, Int. J. Geoinfo. **19**, 13 (2023). https://doi.org/10.52939/ijg.v19i1.2495.
16. S. Avidan and A. Shamir, ACM Transact. Graph. **26**, 1 (2023). https://doi.org/10.1145/1239451.1239461.
17. I. Ashraf, S. Hur, and Y. Park, IEEE Access **5**, 8250 (2017). https://doi.org/10.1109/ACCESS.2017.2699686.
18. W. Burger and M. J. Burge, *Digital Image Processing: An Algorithmic Introduction* (London, Springer Nature, 2022).
19. Y. Liu, M. He, Y. Wang, Y. Sun, and X. Gao, IEEE Access **10**, 95411 (2022). https://doi.org/10.1109/ACCESS.2022.3204657.
20. W. F. Ahmed and M. I. Abd-Almajied, J. Phys.: Conf. Ser. **2857**, 012038 (2024). https://doi.org/10.1088/1742-6596/2857/1/012038.
21. M. I. Abd-Almajied, L. E. George, and K. M. Abood, J. Theo. Appl. Infi. Tech. **97**, 740 (2019).
22. S. Salamon, *Modern Differential Geometry of Curves and Surfaces with Mathematica* (New York, Chapman and Hall/CRC, 2017).
23. A. A. Goshtasby, *Image Registration: Principles, Tools and Methods* (London, UK, Springer Science & Business Media, 2012).
24. E. A. Al-Hilo and R. Zehwar, Int. J. Adv. Comput. Sci. Applicat. (IJACSA) **6**, 112. https://doi.org/10.14569/IJACSA.2015.060518.
25. T. O. Hodson, Geosci. Model Dev. **15**, 5481 (2022). https://doi.org/10.5194/gmd-15-5481-2022.
26. R. S. Hameed and L. E. George, AIP Conf. Proc. **2769**, 020046 (2023). https://doi.org/10.1063/5.0129346.
27. J. T. L. Thong, K. S. Sim, and J. C. H. Phang, Scanning **23**, 328 (2001). https://doi.org/10.1002/sca.4950230506.
28. J. M. S. Ismail, Ibn AL-Haitham J. Pure Appl. Sci. **30**, 237 (2017). https://doi.org/10.30526/30.1.1073.

تحسين جودة دمج الصور باستخدام صور ملونة ذات دقة متعددة

ورود فراس احمد[1] ومحمد اسماعيل عبد المجيد[1]
[1] قسم التحسس النائي ونظم المعلومات الجغرافية، كلية العلوم، جامعة بغداد، بغداد، العراق

الخلاصة
تم استخدام تقنية دمج الصور لتوليد صورة عالية الدقة من صورة منخفضة الدقة. تم تحقيق مقياس عالي عن طريق زيادة دقة الصورة من خلال الاستيفاء، والذي يعتمد على جيران البكسل. تم استخدام صور متعددة الأطياف (صور منخفضة الدقة بدقة عالية) من أقمار صناعية مختلفة في هذا العمل للحصول على صورة عالية الدقة. الجزء الحاسم من دمج الصور هو تسجيل الصورة، والذي يعتمد على الحصول على صورة جيدة عالية الدقة. تم استخدام تحويل الميزة الثابتة للمقياس (SIFT) لاستقبال نقاط التحكم باستخدام تحويل تآلفي. يتم تحديد نقاط التحكم الصحيحة اعتمادًا على مقياس الصورة (خفض المقياس متبوعًا بالرفع)، وهو أمر ضروري لتثبيت نقاط التحكم في المطابقة بين الصور. تم تحديد نقاط التحكم باستخدام خوارزمية SIFT، والتي تستخدم المسافة والزاوية لتحديد نقاط المطابقة الصحيحة. يتم استخدام صورة بمقياس مختلف للكشف عن نقاط التحكم الصحيحة بين الصورتين ومطابقتها، وبالتالي تسريع العملية. كما استُخدمت تقنية تحجيم الصورة مع تمديد التباين في المعالجة المسبقة لتمديد السطوع للحصول على خصائص صورة عالية الجودة. وتُطبّق عملية مورفولوجية على الصور بعد المعالجة (تحجيم، تمديد التباين، وعملية قياس الإشعاع). ويتم الحصول على دمج الصورة النهائي باستخدام نموذج اللون (السطوع، والصبغة، والتشبع). ويُستخدم معيار متري، وهو جذر متوسط مربع الخطأ (RMSE)، مع نسبة ذروة الإشارة إلى الضوضاء (PSNR)، لتحديد جودة هذه العملية المستخدمة في دمج الصور.

الكلمات المفتاحية: صورة مدمجة، صورة عالية الدقة، صورة منخفضة الدقة، صورة طيفية متعددة، مطابقة صورة.